JGR Solid Earth

RESEARCH ARTICLE
10.1029/2022JB024668

Episodic Venting of a Submarine Gas Seep on Geological Time Scales: Formosa Ridge, Northern South China Sea

Pascal Kunath[1,2,3], Gareth Crutchley[1], Wu-Cheng Chi[2], Christian Berndt[1], Char-Shine Liu[3], Judith Elger[1], Dirk Klaeschen[1], and Gerhard Bohrmann[4]

[1]GEOMAR Helmholtz Centre for Ocean Research Kiel, Kiel, Germany, [2]Institute of Earth Sciences, Academia Sinica, Taipei, Taiwan, [3]Ocean Center, National Taiwan University, Taipei, Taiwan, [4]Department of Geosciences / MARUM - Center for Marine Environmental Sciences, University of Bremen, Bremen, Germany

Abstract The Formosa Ridge cold seep is among the first documented active seeps on the northern South China Sea passive margin slope. Although this system has been the focus of scientific studies for decades, the geological factors controlling gas release are not well understood due to a lack of constraints of the subsurface structure and seepage history. Here, we use high-resolution 3D seismic data to image stratigraphic and structural relationships associated with fluid expulsion, which provide spatio-temporal constraints on the gas hydrate system at depth and methane seepage at modern and paleo seafloors. Gas has accumulated beneath the base of gas hydrate stability to a critical thickness, causing hydraulic fracturing, propagation of a vertical gas conduit, and morphological features (mounds) at paleo-seafloor horizons. These mounds record multiple distinct gas migration episodes between 300,000 and 127,000 years ago, separated by periods of dormancy. Episodic seepage still seems to occur at the present day, as evidenced by two separate fronts of ascending gas imaged within the conduit. We propose that episodic seepage is associated with enhanced seafloor sedimentation. The increasing overburden leads to an increase in effective horizontal stress that exceeds the gas pressure at the top of the gas reservoir. As a result, the conduit closes off until the gas reservoir is replenished to a new (greater) critical thickness to reopen hydraulic fractures. Our results provide intricate detail of long-term methane flux through sub-seabed seep systems, which is important for assessing its impact on seafloor and ocean biogeochemistry.

Plain Language Summary Gas hydrates are ice-like compounds that form in marine sediments. They can reduce the permeability of the sediments by clogging up the pore spaces, and influence how methane gas flows through sediments and then seeps out of the seafloor. Seepage of methane into the water column plays an important role in seafloor biology and ocean chemistry. In this study, we use 3D seismic imaging to investigate the subseafloor sediments of a ridge in the South China Sea where gas is currently seeping into the ocean. Our data show, in high detail, how gas migrates upward through the sediments due to the buoyancy of gas. Our data also reveal mound structures at certain depths beneath the seafloor. We interpret that these mounds represent distinct phases in the geological past where gas was seeping out of the seafloor. This indicates that gas seepage at this ridge has switched on and off (episodically) throughout geological time. We speculate that the episodic seepage is associated with rapid seafloor sedimentation, which changes pressure conditions beneath the seafloor. Our work improves the understanding of how gas seepage processes can change on geological timescales.

Key Points:

- Gas has accumulated beneath the base of gas hydrate stability, causing vertical gas conduit formation and seabed mounds
- Mounds imaged within the conduit record episodic seepage between 300 and 127 kyrs ago
- Quiescence may be associated with enhanced seafloor sedimentation that increases effective stress at the top of the gas reservoir

Supporting Information:

Supporting Information may be found in the online version of this article.

Correspondence to:

P. Kunath,
KunathPascal@gmail.com

Citation:

Kunath, P., Crutchley, G., Chi, W.-C., Berndt, C., Liu, C.-S., Elger, J., et al. (2022). Episodic venting of a submarine gas seep on geological time scales: Formosa Ridge, northern South China Sea. *Journal of Geophysical Research: Solid Earth*, *127*, e2022JB024668. https://doi.org/10.1029/2022JB024668

Received 26 APR 2022
Accepted 28 AUG 2022

Author Contributions:

Conceptualization: Pascal Kunath, Gareth Crutchley
Formal analysis: Pascal Kunath, Gareth Crutchley, Wu-Cheng Chi
Funding acquisition: Wu-Cheng Chi, Christian Berndt, Char-Shine Liu
Investigation: Pascal Kunath, Gareth Crutchley, Christian Berndt
Methodology: Pascal Kunath, Dirk Klaeschen
Resources: Wu-Cheng Chi
Software: Pascal Kunath
Validation: Pascal Kunath
Visualization: Pascal Kunath

1. Introduction

The high-pressure and low temperature conditions in deep-water environments (>300–500 m) cause hydrocarbon-rich fluids to form ice-like compounds of gas hydrate in the sediment pore space (Sloan & Koh, 2007). These pressure and temperature conditions, together with appropriate salinity and adequate supply of gas and water, confine gas hydrates to the upper few hundred meters of sediments—the gas hydrate stability zone (GHSZ). The formation of gas hydrates directly above the base of the GHSZ (BGHSZ) reduces the permeability of the host sediment as it clogs up the pore spaces (e.g., Fang et al., 2020). Thus, large gas hydrate deposits may form laterally extensive seals at the BGHSZ. This, in addition to the fact that free gas forms solid methane hydrate once it mixes with water inside the GHSZ (Haeckel et al., 2004), as well as authigenic carbonate formation by anaerobic oxidation of methane (AOM) near the seafloor that can plug fluid flow pathways (Tréhu et al., 2004b), means that fluids do not always easily migrate through the GHSZ (e.g., Liu et al., 2019; Liu & Flemings, 2006;

Writing – original draft: Pascal Kunath, Gareth Crutchley
Writing – review & editing: Wu-Cheng Chi, Christian Berndt, Char-Shine Liu, Judith Elger, Dirk Klaeschen, Gerhard Bohrmann

Milkov et al., 2005). Likewise, the existence of different lithologies within the GHSZ, such as low-permeability mass transport deposits (Sawyer et al., 2009), can also thwart upward fluid flow and result in complex spatial distributions of gas hydrate and free gas (Crutchley et al., 2021).

Cold seeps are frequently documented in gas hydrate provinces (e.g., Talukder, 2012 and references therein), including in the South China Sea (Feng et al., 2018). Cold seeps are locations at the seafloor where mostly methane-rich fluids are released into the overlying water column. The emanating fluids can lead to various seabed features, such as authigenic carbonate deposits, sedimentary mounds, chemosynthetic communities, reduced sediments and pockmarks (e.g., Judd & Hovland, 2009; Koch et al., 2016; Levin et al., 2016; Liebetrau et al., 2010). While surface structures of cold seeps have been well described (e.g., Talukder, 2012), there is much less known about the different styles of fluid pathways at depth. Seismic reflection imaging has shown that their underlying plumbing system often changes from layer-constrained beneath the BGHSZ to sub-vertical focused fluid flow through the GHSZ (Crutchley et al., 2013; Hustoft et al., 2010; Tréhu et al., 2004a). Focused flow through the GHSZ often manifests itself as columnar zones of disrupted reflection continuity. These focused fluid flow structures, variably termed chimneys, pipes or conduits, initiate at pressure foci, such as the topographic high of the bottom-simulating reflection (BSR; Shipley et al., 1979)—the reflection resulting from the seismic impedance contrast between hydrate filled sediments above and a zone containing free gas below the BGHSZ. Due to this contextual link to the focus of overpressure, their formation is commonly attributed to breaching of top seals by hydraulic fracturing under elevated pore pressures (Cartwright et al., 2007; Flemings et al., 2003; Tréhu et al., 2004a). Focused fluid flow then occurs through near vertical zones of fractures that permit flow through the GHSZ. In this paper we refer to these sub-vertical focused fluid flow pathways as "conduits".

Identifying the processes controlling seepage distribution, pulses, and duration is important for assessing its impact on ocean biogeochemistry and seabed chemosynthetic communities that feed directly from methane seeps (Milkov et al., 2005; Valentine, 2011). Previous studies have shown that seepage activity can vary both in time and in space (Kannberg et al., 2013; Plaza-Faverola et al., 2011; Suess et al., 2001). However, the underlying geological mechanisms leading to spatial-temporal variability of gas seepage often remain elusive, and there are a number of important interrelationships that need to be considered between processes including hydrate formation dynamics, authigenic carbonate precipitation, and focused flow along faults, fractures, and high-porosity lithologies (Crutchley et al., 2013; Milkov et al., 2005; Teichert et al., 2003; Tréhu et al., 2004a). In addition, typical geological archives, such as seep carbonates (e.g., Han et al., 2014; Nyman et al., 2010), may only reveal partial stages of fluid seepage, while identifying seepage histories from seismic data is difficult because fluid migration patterns are typically concealed by poor image quality at depth and/or overprinting from successive gas migration episodes. Still, seismic images can potentially provide spatial relationships that could be linked to time constraints by seismic stratigraphy. The difficulty in carrying out such studies is obvious, as it requires high quality 3D seismic data that can reveal the sub-seafloor architecture, ideally down to sub-seafloor depths greater than the BSR depth, in meter-scale resolution.

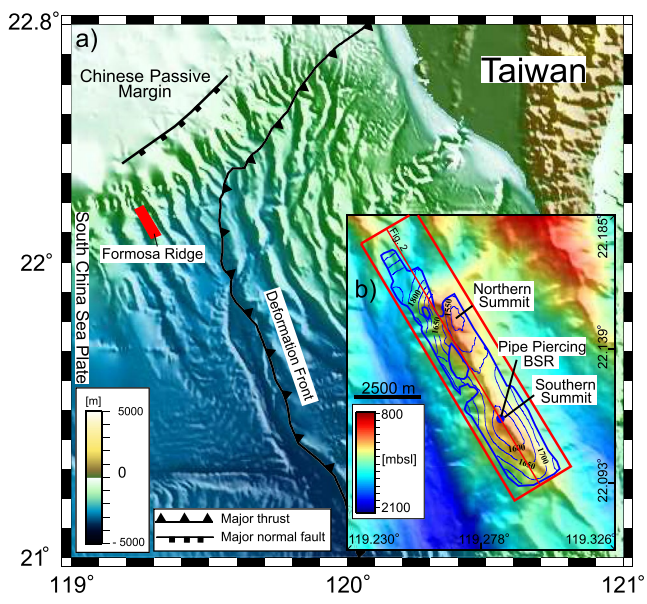

Figure 1. (a) Regional map. Red box displays survey area. Formosa Ridge represents one of the topographic ridges created by canyon incision in the area. (b) 75-m resolution bathymetry map of the study area. On top of the bathymetry, red outline shows the bounding box of the 3D seismic volume. Blue bold polygons highlight the area where we mapped the bottom-simulating-reflection (BSR). Blue contour lines show the depth of the BSR in meters below sea-level. Blue circle marks the intersection of the BSR and conduit, which is slightly toward the northwest of the local topographic high of the BSR surface.

Here, we use high-resolution P-Cable 3D seismic data to provide new insight into the sub-seafloor architecture of the Formosa Ridge gas conduit in the South China Sea (SCS; Figure 1). Our aim is to characterize the stratigraphic and structural expression of fluid expulsion, and its spatio-temporal relationship with the gas hydrate system at depth and methane seepage at the seafloor. The 3D seismic data provide higher horizontal (3 × 3 m) and vertical (3–5 m) resolution of the top 500 mbsf, compared with industry-acquired conventional 3D seismic, allowing the gas conduit structure to be imaged in great detail. This dataset provides a better understanding about gas hydrate systems, including their dynamics and related focused fluid flow in three dimensions. The data enable us to propose a model for seepage evolution during the last 300,000 years.

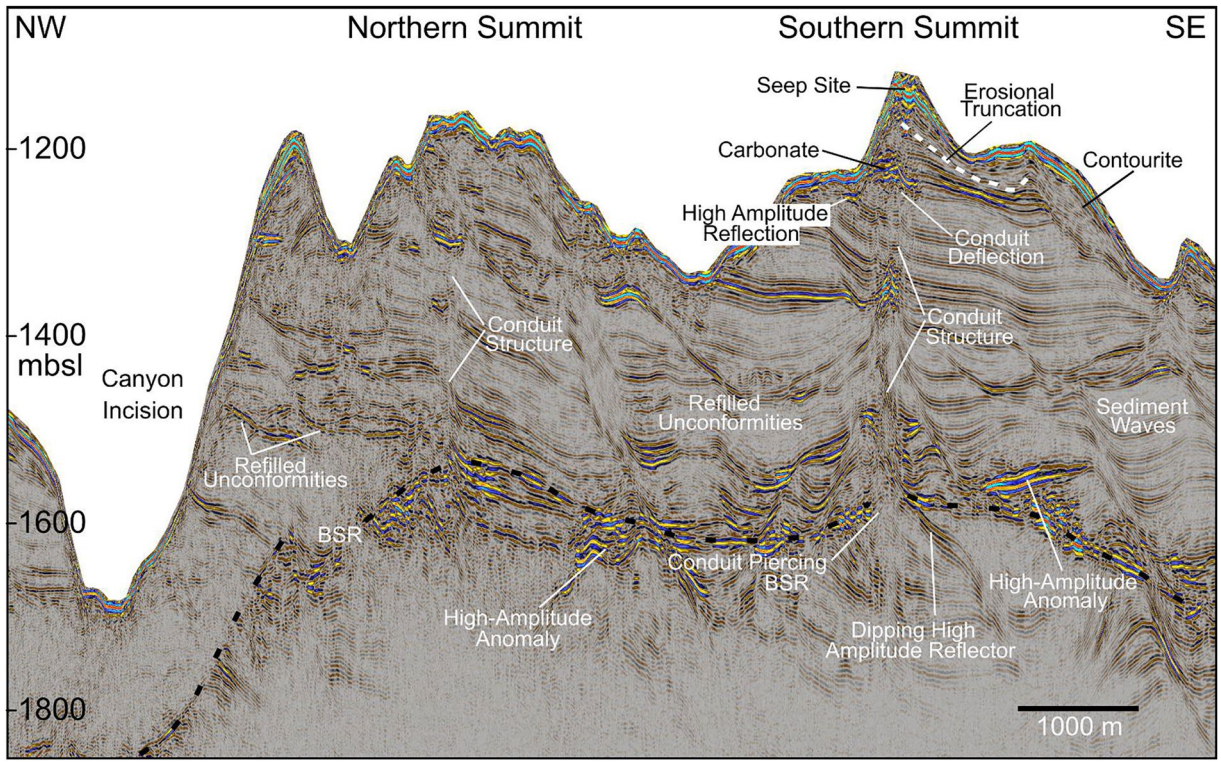

Figure 2. Arbitrary line extracted along the crest of Formosa Ridge from the high-resolution 3D seismic volume. Line location is shown in Figure 1b. The interpreted BSR is marked by the broken black line. It manifests itself in general as a high amplitude reflection with reverse seismic polarity, mimicking the bathymetry of the modern seafloor and cross-cutting some sedimentary strata. Note: the BSR is not always continuous, and is sometimes picked as the upper limit of strong reflectivity caused by free gas beneath the hydrate stability zone.

2. Previous Research and Geological Setting

The study area is on the passive margin on the northern continental slope of the SCS, about 100 km west of Taiwan (Figure 1a). The active cold seep is on the southern summit of Formosa Ridge (Figure 1b), a contourite drift created by canyon incision, similar to the other NNW-SSE trending topographic ridges in the region. The canyons are up to 700 m deep, carved by turbidity currents.

The Formosa Ridge cold seep site is among the best-studied seep sites on the northern SCS passive margin slope. It is the only known active seep site there (Feng & Chen, 2015; Han et al., 2014; Tong et al., 2013) and has therefore been studied using different geological and geochemical approaches to understand its seepage history and the driving mechanisms for gas flow (Feng & Chen, 2015; and references therein). Feng and Chen (2015) suggested initiation of methane seepage from at least 10.6 ka BP based on ^{14}C dating of carbonate samples retrieved at the seafloor. Moreover, the samples yielded ages of seepage periods of varying intensities at time scales of thousands of years, when sea level was relatively stable. Thus, effects of hydrostatic pressure to trigger seepage events seem to be irrelevant at this site, which has been proposed to be in contrast to the other seep environments in the region, where U/Th dating of seep carbonates corresponded to times of falling or low sea level (Feng et al., 2018). The chronology of seepage at Formosa Ridge throughout its geological history remains unknown.

Due to the lack of drilling information, the lithostratigraphy of Formosa Ridge is poorly defined. Thus, the subsurface structure of Formosa Ridge is known mostly from seismic reflection imaging. Seismic facies mapping suggests that the ridge's deposits have been reworked by sedimentary-gravity flows, including canyon/channel erosion, turbidity flow spilling and slumping (Berndt et al., 2019; Fongngern et al., 2022). The northern part of the ridge has been more affected by erosional processes as evidenced by canyon-fill deposits, while the southern area is mainly composed of sediment wave deposits (Figure 2, Berndt et al., 2019). Two distinct gas conduits were identified beneath the northern and southern summits. The conduit beneath the southern summit, which connects to the active cold seep site at the surface, is the focus of this study. The conduit intersects the local topographic

high of the BSR, suggesting that a permeability boundary and/or capillary sealing at the BGHSZ leads to gas accumulation (Berndt et al., 2019). Overall, the BSR is well-defined and continuous beneath the entire ridge (Figure 1b).

Scientific drilling of Formosa Ridge was undertaken in 2018 using MARUM's remote seafloor drill rig MeBo 200 (Bohrmann et al., 2019). The cold seep site at the southern summit of the ridge was drilled and cored to ∼126 mbsf. Authigenic carbonates were sampled in both the near surface sediments and at ∼91 mbsf, indicating a long-lived seep system.

3. Methods

3.1. 3D Seismic Data

The seismic volume was acquired with GEOMAR's P-Cable system (Planke et al., 2009) during the cruise SONNE 227 (Berndt et al., 2019). The system consisted of an array of 14 streamers (25 m long) with eight receiver groups. GPSs receivers were attached to each paravane and to a known position on the ship for reference. The source was a GI gun firing every 5 s at 21,000 kPa (210 bars), equivalent to ∼7 m shot spacing at an approximate ship speed of 1.8 m/s. The record length was set to 4 s at a sampling rate of 1 ms and the signal frequency ranges between 50 and 180 Hz.

The seismic processing workflow was established with the software OMEGA2 from Schlumberger, following in general that which was outlined in Berndt et al. (2019) and Kunath et al. (2020). The flow consisted of following main steps: (a) navigation quality control (b) calculation of the streamer and channel position geometry (see Petersen et al. (2010), (c) trace editing/removal and back interpolation from neighboring traces along dips of maximum coherency, (d) static time corrections, (e) band-pass filtering (low cut frequency 50 Hz), (f) noise burst removal in the shot gather domain with overlapping 3D time-space windows using average spectral amplitude threshold ratios from three neighboring streamers, (g) random noise, coherent noise and swell noise suppression in the shot gather domain by a 3D dip-filter in the F-X-Y domain for each frequency slice of the data, (h) linear Radon transform dip-filter to increase the reflection continuity along each single streamer, (i) common-midpoint sorting and hyperbolic move-out corrections with an OBS-derived velocity field (Berndt et al., 2019) and stacking the cube in 3.125 × 3.125 m bins, (j) trace interpolation in the in-line and (subsequently) cross-line directions to fill data gaps along dips of maximum coherency, (k) poststack 3-D F-K coherency filter to obtain spatial continuity, (l) Stolt migration with a constant velocity of 1,500 m/s followed by a residual finite difference time migration and a time to depth conversion using a smoothed velocity field derived from the ocean-bottom seismometer (OBS) data. The OBS derived velocities increase from less than 1,600 m/s at the seafloor to 1,800 m/s at about 300 ms TWT below the seafloor and up to 1,850 m/s directly above the BSR (for further details see Berndt et al. (2019)). The depth migrated seismic volume has a lateral resolution of 3.25 m and a vertical resolution of ∼5 m (i.e., taken as λ/2), with a maximum fold of 31 and an average fold of 4.

3.1.1. 3D Seismic Attributes

We characterize the 3D architecture of the conduit by visualizing and interpreting local stratigraphic and structural differences, in addition to indications of subsurface fluids appearing at different stratigraphic levels. The interpretation is carried out using IHS Kingdom software.

Seismic attributes are quantities derived from the seismic data that describe the shape or other characteristics of a seismic trace over a specified depth interval (e.g., Chopra & Marfurt, 2007; Taner, 1997). We derived seismic attributes from a single trace by comparison of multiple traces, and from an interpreted seismic horizon to map structural features such as fractures, depositional features such truncation of strata, and amplitude anomalies to characterize fluid migration patterns:

We calculated Root-Mean-Square (RMS) amplitude volumes to highlight seafloor seeps, gas accumulations and carbonate precipitations, which are manifested as high RMS amplitudes. The rather young and weakly consolidated sediments in the shallow subsurface manifest themselves as low RMS due to relatively low impedance contrasts. RMS amplitudes were calculated within depth windows of 25–75 m, centered at specific surfaces that we picked within the 3D seismic data.

The similarity attribute (i.e., a measure of coherency that represents the degree of spatial continuity along a reflection, e.g., Crutchley et al., 2013) is calculated using a vertical aperture of 50–100 m to highlight high angle, vertically persistent fractures and dipping flanks of the conduit.

We calculated a zero-crossing attribute to highlight changes in depositional patterns associated with the flanks of the conduit. Specifically, we map truncations of the seismic horizons associated with the conduit's flanks. Zero-crossing attribute calculates the number of zero crossings of the seismic trace within a specific depth interval above the base of the investigated stratigraphic unit. As such, it can highlight depositional pattern differences inside the conduit for wavelengths equal to the vertical resolution of the data (in our case ~5 m). We interpret such truncations of horizons as marking the deposition of sediment layers against buried seabed geomorphological features, such as carbonate mounds and/or regions of sediment deformation caused by past periods of vigorous fluid expulsion (e.g., Plaza-Faverola et al., 2011). As such, horizon truncations can be useful chronological markers of fluid expulsion.

3.2. Seismic Chrono-Stratigraphy

In the absence of direct chronostratigraphic calibration from boreholes for the sedimentary units deeper than 91 mbsf at the southern summit, we used average sedimentation rates (0.7 m/ka) from the MeBo-drill core to constrain the chrono-stratigraphy of prominent horizons and sedimentary units. We use a nomenclature where "H" stands for Horizon and "T" stands for thickness map of individual sedimentary units.

4. Results

4.1. Seismic Character of the Conduit

The seismic section extracted from the 3D data in Figure 2 highlights the sub-seafloor stratigraphic reflections, the conduit structure, the BSR, and prominent anomalous high amplitude reflections beneath and within the GHSZ. The most conspicuous feature of Formosa Ridge is the conduit located underneath the southern summit of the ridge.

The conduit manifests itself in constant depth slices of the data as a circular to elliptical zone (200–350 m diameter) of disrupted reflectivity (e.g., Figures 3 and 4), from the seafloor down to 700 mbsf—the seismic penetration limit of this dataset. Reflection amplitudes within the conduit are highly variable, with localized high amplitude anomalies distributed 91 m below the summit and at 100 and 250 m above the BGHSZ (Figure 3a). Those amplitude anomalies can be the result of either high concentrations of gas hydrate, free gas, or carbonate precipitates. Drilling results from the Expedition SO266 (Bohrmann et al., 2019) revealed that the normal polarity bright spot at 91 m below the summit represents a ca. 5m-thick layer with carbonate nodules that formed 127 ka years ago. It has a diameter of ~320 m in the seismic data, lies sub-horizontally (1–4° dip), and extends toward the northwest where it almost intersects the seafloor at the southern summit of the ridge (Figure 3b, and c). The origin of the two bright spots located in the deeper part of the conduit could not be ground-truthed through drilling. To elucidate their nature, we therefore compare their seismic characteristics with those from areas where the nature of high amplitude reflections are well constrained. In contrast to the layers of authigenic carbonates above, the two bright spots occur over a larger depth interval of 40–75 m (Figure 3a), exhibit relatively chaotic and scattered reflections (Figure 3b) and show smaller diameters of about 200 m (Figure 3d, and e). Furthermore, the depth interval that separates the two bright spots shows significantly reduced reflectivity, while the reflections above and below the carbonate patch are more coherent. We have analyzed the frequency/wavenumber content of the seismic data, as it can help to identify free gas in the sediments, because the presence of free gas in pore space absorbs the high frequency component of the seismic energy (e.g., Taner, 1997; Taylor et al., 2000), translating to lower frequency and smaller wavenumber compared with that outside of the conduit at similar depths. Results show lower dominant wavenumbers below the first and second bright spots (blue and black boxes, Figure 3b), which is not observed at the shallower depths beneath where the authigenic carbonate nodules were sampled (red box, Figure 3b).

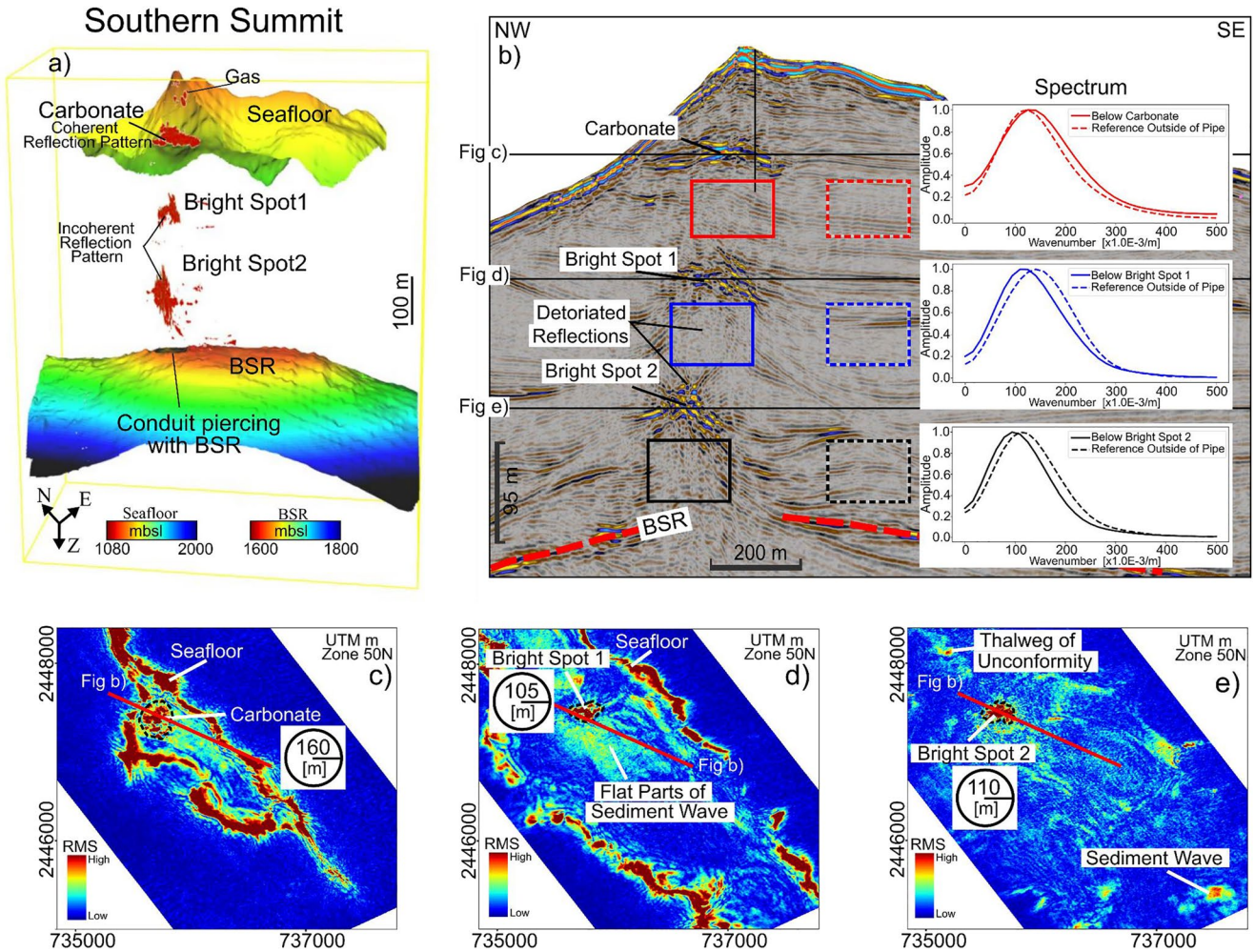

Figure 3. (a) Volume rendering of the RMS amplitude attribute cube showing only the brightest features between the BSR and southern summit of the ridge. Most of the high amplitudes occur within the conduit. (b) Spectra calculated for different depth windows (red, blue and black boxes) above and below the bright spots inside the conduit. For reference, we also calculate spectra beyond the conduit in regions (broken boxes) that are not affected by amplitude anomalies. With respect to the reference regions (broken boxes), the dominant wavenumber is decreased below the bright spots (blue and black windows), in contrast to the region beneath the carbonate deposit (red window), where the dominant wavenumber is increased with respect to the reference region. Black vertical line shows the location and depth range of the Mebo drill hole (Bohrmann et al., 2019). (c)–(e) Depth slices of the RMS amplitude attribute cube at 1,230, 1,355, and 1,475 mbsl, respectively. Circular to elliptical features can be clearly identified. The Bright spots have a diameter of 105–110, while the carbonate crusts' diameter is 160 m. Coordinate system (in meters) is UTM Zone 50N, WGS84 datum.

4.2. Fracture Characteristic

The fractured regions (e.g., near vertical features with no evident vertical displacement along reflections) inside the conduit are illuminated as streaks of low similarity between the summit and the maximum imaged depth (Figure 4). The fracture characteristic changes with depth. We mapped high-density fracture distribution between H8 (~200 m below the modern BSR) and H0 (authigenic carbonate formation). Within this depth interval, digitized conduit perimeters extracted from similarity slices from various horizon depths (H0, H1, H3, H5, and H8) show a persistent conduit location and a vertical conduit geometry (Figures 4c–4e). However, at a smaller scale, branching of the conduit is observed at the depth of H3 (Figure 4a). Lateral deflection of fractures occurs directly beneath the carbonate layer at H0; the deflection extends approximately 100–200 m toward the south (Figure 4g, and h). Thus, fractures do not extend strictly vertically from beneath the modern BSR toward the seafloor. Intriguingly, it is within this shallow depth interval between the seafloor and H0 that we observe the fracture density distribution decreasing. It seems fewer fractures extend from depth across the carbonate patch into the near-surface sediments.

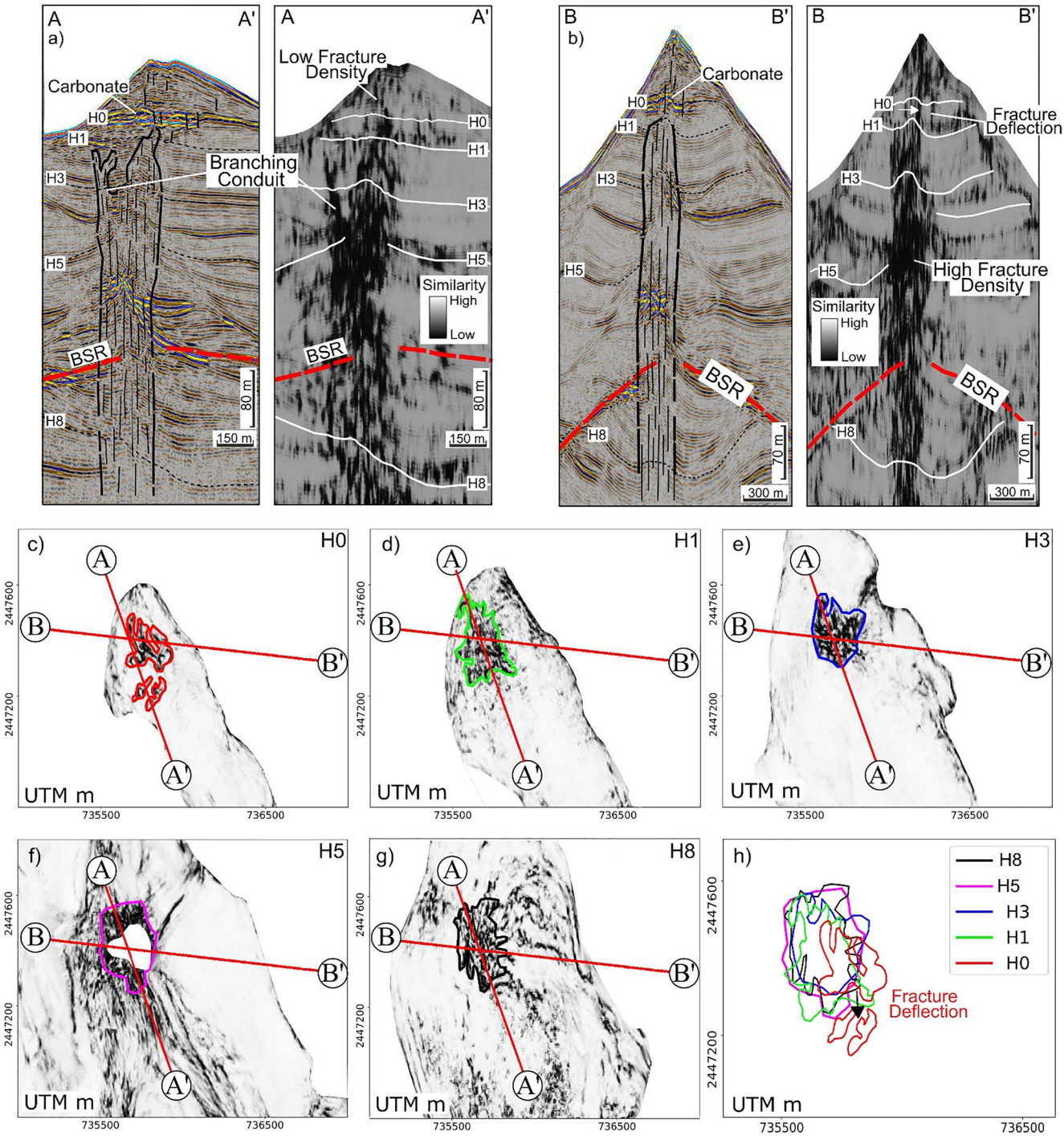

Figure 4. (a) and (b) Arbitrary lines (A to A' and B to B') extracted along the crest of Formosa Ridge from the high-resolution 3D seismic data. Similarity attribute highlights the fine-scale (>10 m width) near-vertical fracture zones imaged within the Formosa Ridge conduit. Note that fractures zones branch laterally at H3, approximately 100 m away from the center of the conduit. (c)-(g) Similarity slices from five sub-seafloor horizons (H0, H1, H3, H5, and H8) are presented to show the conduit planform geometries at different depths. Note: coordinate system (in meters) is the same as in Figure 3 (h). Digitized conduit perimeters from various depths showing conduit planform shape and spatial location change with depth. The conduit location has been relatively stable throughout its formation, until reaching H0, from where it is deflected toward the southeast.

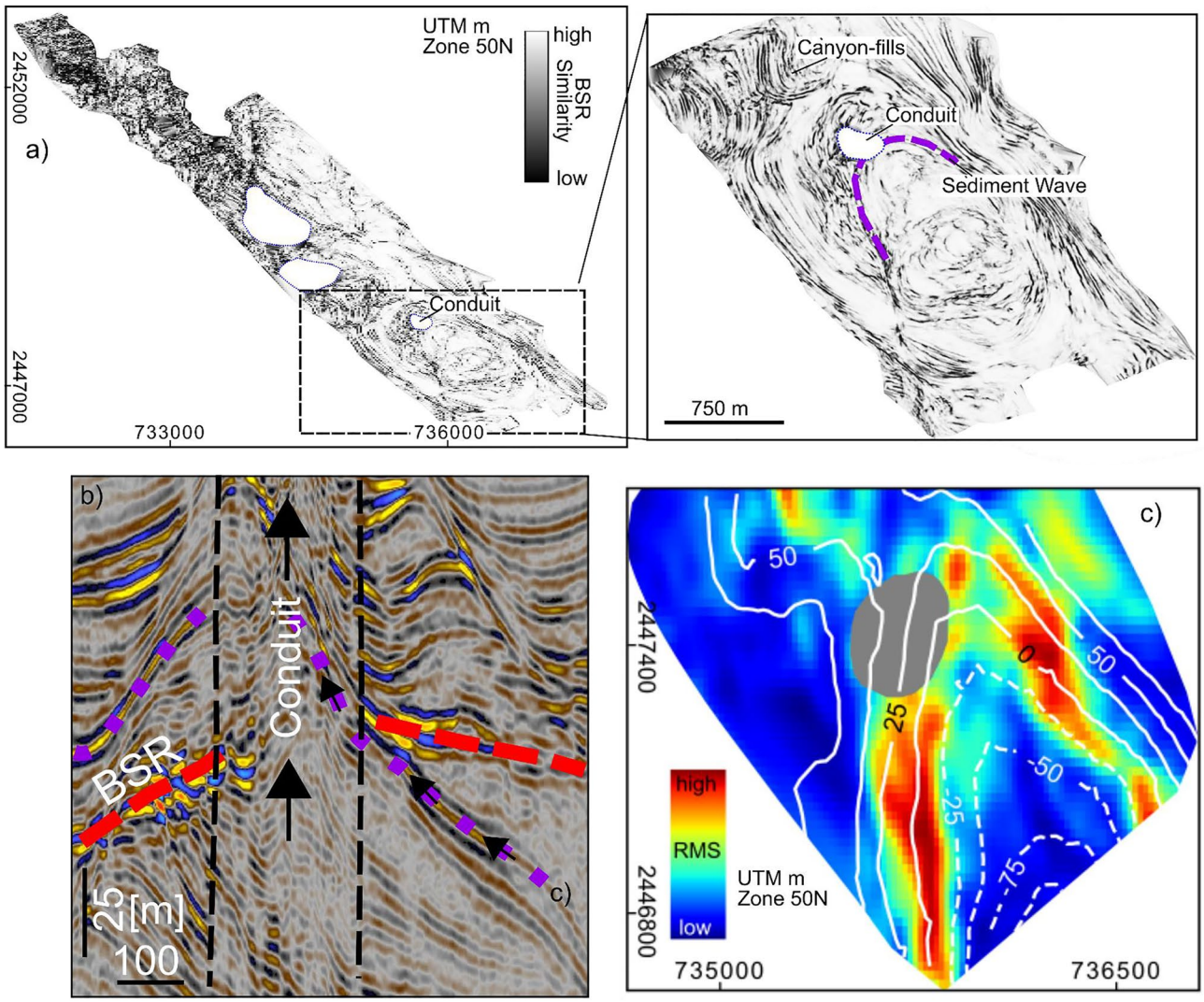

Figure 5. (a) Seismic similarity of the bottom simulating reflection (BSR). Purple dashed line in the enlargement to the right is our interpretation of the sediment wave-BSR intersection. The region of low similarity northwest of the conduit is caused by fabrics of wavelet tuning where canyon-fill strata intersect with the BSR. (b) Interpreted seismic section in the region around the intersection of the conduit with the BSR. High amplitude reflections crossing the BSR mostly follow the stratigraphy of dipping sedimentary layers. Dotted purple line is a sediment wave reflection that intersects the BSR in the region where the conduit is located (see also the enlargement in (a)). Vertical black arrows indicate vertical gas flow through the conduit. (c) Amplitudes on the sediment-wave horizon shown by the dotted purple line in (b). Depth contours are meters above and below the BSR, positive and negative numbers, respectively. Gray region is where the conduit is. We interpret that the more steeply dipping strata of the sediment wave enhances gas migration upward into the GHSZ.

4.2.1. Geological Structures and BSR

We analyzed prominent structures crossing the BSR (Figure 5a). Structures on the BSR in close proximity to the conduit, determined from the similarity attribute, are primarily a result of (a) fractures (as mentioned above); and (b) crosscutting stratigraphic sequences, for example, sediment-wave reflections in the southeast and cut and fill deposits in the northwest. The location of the conduit coincides with the intersection of the BSR with the top of a prominent sediment wave package (Figure 5b). This relationship is well described in a map of the top of the sediment wave package shown in Figure 5c, showing relative depth contours with respect to the BSR, and RMS amplitudes. Figure 5c shows that anomalously high reflectivity is conformable with this sediment wave layer, and that the vertical extent of the sediment wave above the BGHSZ is about 25–50 m. In contrast, high amplitude reflections crossing the BSR are not observed along the fractures imaged in the seismic data (Figure 4a, and 4b).

4.3. Timing of Conduit Formation or Re-Activation

Mapping truncations of seismic horizons against the conduit can provide insight into the temporal nature of the conduit formation. This approach is based upon both sediment doming and authigenic carbonate formation occurring at the seafloor, which is to be expected (Koch et al., 2016; Tréhu et al., 2004b). Figures 6a and 6b show where we have mapped upward doming (mounds) within the conduit (broken white lines), that is, above H3, H1.3, and H1. The mounds at H3 and H1 occur within the main conduit, while the mound at H1.3 is above the branching conduit. The maximum amount of doming at the mounds is 20 and 10 m for the H3 and H1 horizons, respectively (Figure S1 in Supporting Information S1), indicating a reduction of surface doming with later fluid expulsion episodes. The inferred formation times for the buried mounds inside the conduit are 298 ± 213 ka, 220 ± 116 ka, and 183 ± 70 ka for H3, H1.3, and H1, respectively, using the average sedimentation rates extrapolated from MeBo drilling (Figure 6c).

Figures 6d–6f shows zero crossing attribute maps of the three major stratigraphic intervals where truncations are observed. The scale represents the number of zero crossing within a specified depth window above the respective horizon. Truncations are indicated by a sudden decrease in number of zero crossings because it removes at least one full phase from the seismic signal. The background number of zero-crossings for the specified depth window above H1 (refer to zc1 in Figure 6b) is >8, which corresponds to the regions where conduit related depositional patterns are absent (Figure 6d). In contrast, truncation of reflections against the conduit causes a pronounced decrease (to <8) in the number of zero crossings of the seismic signal. We observe a similar pattern for the depth interval above H1.3 (zc2)–a drop of zero-crossing number from the background number >3 to <3 at the intersection with the conduit (Figure 6e). For the depth interval above H3 (zc3), a drop to a lower zero-crossing number (<3) indicates termination of reflectors toward the conduit or non-uniform deposition (i.e., on the lee side of sediment-wave like features) (Figure 6f).

4.4. Laterally Varying Depositional Patterns Coinciding With Conduit Formation Times

To test whether a spatial and temporal correlation exists between depositional patterns and conduit formation, we characterized the stratigraphic units coinciding with the previously identified fluid expulsion periods (i.e., the mound ages). Three units are described from bottom to top (Figures 7a–7d): T3, T2, and T1. Within unit T3 and T2, canyon fill and sediment wave deposits coincide with the conduit location toward the northwest and the southeast, respectively (Figure 2). In a stratigraphic sense, T3 and T2 were deposited before the conduit structure was formed, or reactivated 298 ka BP, while unit T1, which consists of relatively condensed contourite deposits, was deposited later.

The sedimentation pattern reconstruction highlights strong laterally varying sedimentation between units T3 and T2. Unit T3 sediment depocenters (150–220 m thick) exist in the east and southeast relative to the conduit location, which is 3–6 times the thickness observed in the northwest (Figure 7b). In contrast, for unit T2, maximum sediment thickness increases up to 170–190 m toward the west and north (Figure 7c), while toward the southeast sediment thickness decreases by a factor of five compared to unit T3. Thus, the depositional regime has changed substantially between the two units, with sediment depocenters moving from the southeast toward the north and northeast. Relative to Units T2 and T3, the sediment thickness in the vicinity of the conduit for T1 remains relatively constant, with a localized thickness variation of less than a factor of 1 (Figure 7d).

5. Discussion

5.1. Internal Sediment Deformation: Multiple Cycles of Pressure Build-Up and Release or an Imaging Artifact?

Formation or reactivation of focused fluid conduits can manifest as onlap of the reflectors onto buried seabed geomorphological features that have formed due to vigorous release of overpressured fluids. Fluid escape conduits in the Nyegga area, off Norway, are a well-documented example, where episodic conduit growth is inferred seismically from mapping of seabed doming structures (Plaza-Faverola et al., 2011). Other examples of seafloor doming due to gas ascent have been documented elsewhere (e.g., Koch et al., 2016; Passaro et al., 2016). However, the seismic interpretation of such seabed doming features when buried within a gas conduit can be difficult due to transmission and velocity artifacts generated by structures with anomalous impedance contrasts

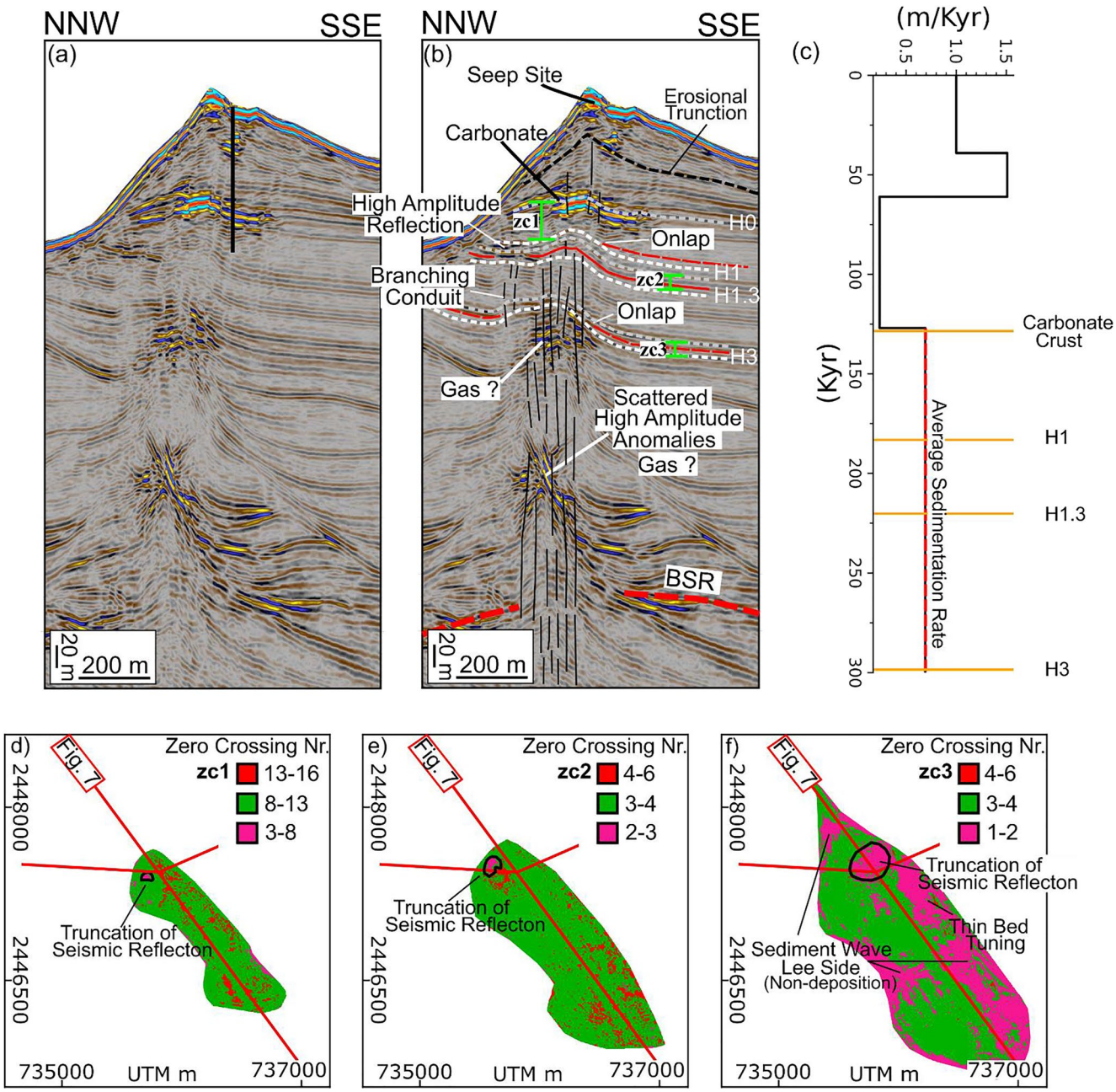

Figure 6. (a) 2D extraction of seismic data along the southern summit of the ridge, showing the Formosa Ridge conduit. Black vertical line shows the location and depth range of the Mebo drill hole (Bohrmann et al., 2019). (b) Interpreted seismic section. White dashed lines highlight the surfaces where we mapped paleo-seafloor mounds. Onlap (thin dashed red lines) indicate truncated reflections toward the conduit. The supplementary material Figure S1 and S2 in Supporting Information S1 show further examples of truncated reflections against the conduit. zc1, zc2 and zc3 refer to zero-crossing attribute windows (green bars) used to extract the maps shown in (d), (e) and (f), respectively. (c) Sedimentation rates at the site for the last 300 kyrs, together with the timing of mound formation (horizontal orange lines). Sedimentation between 127 ka and 300 ka was extrapolated using average sedimentation rates constrained by MeBo drilling (Bohrmann et al., 2019). The reader is referred to Supporting Information S1 for assessments of uncertainty in depths of key horizons. (d)–(f) Zero crossing maps of the three major stratigraphic intervals where truncations are observed. The scale represents the number of zero crossing within a specified depth window above the respective horizon (see green bars in (b)). Truncations are indicated by a sudden decrease in the number of zero crossings.

in the shallow marine section, such as carbonates (Judd & Hovland, 2009). Carbonates have been documented in our dataset (Bohrmann et al., 2019, Figure 3a). Fortunately, in the example presented here, we have the possibility to map the conduit's internal structure and adjacent stratigraphy in 3D and at very high resolution (Figure 6). The presence of paleo-seafloor mounds at different stratigraphic depths within the single conduit, and associated

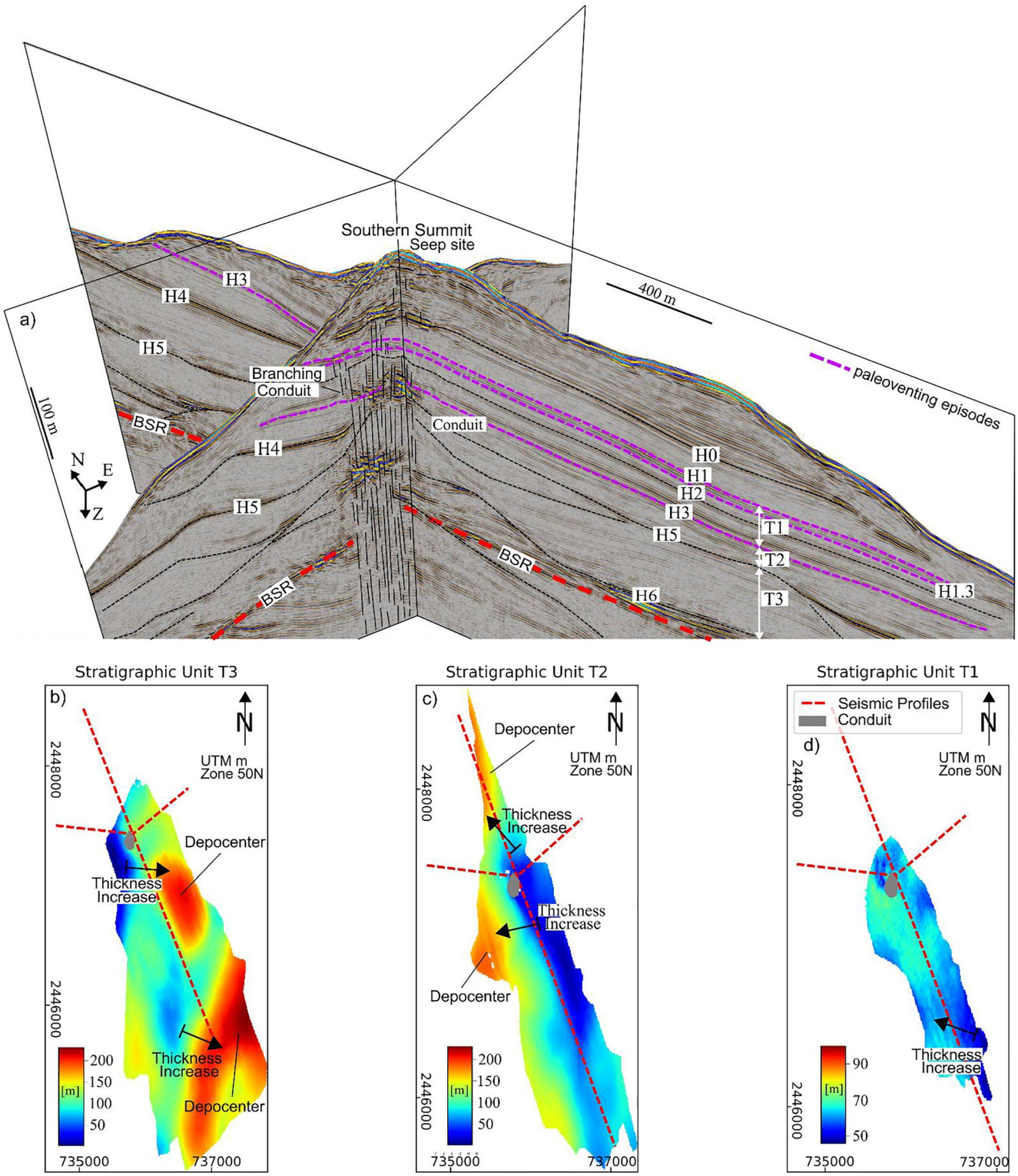

Figure 7. (a) Arbitrary seismic lines across the southern summit. (b)–(d) Thickness maps for units T3, T2 and T1, respectively, indicated in the seismic profiles in (a). The dashed red lines indicate the locations of the seismic profiles shown in (a). The arrows point toward regions of maximum thickness increase. Gray filld polygons mark the location of the conduit on these thickness maps.

truncated reflectors against their flanks, are critical observations to rule out acoustic artifacts. The deformed (up-bending) reflections against the conduit cannot be explained by velocity pull-up effects from overlying high seismic velocity material (e.g., Hornbach et al., 2012), since such a velocity artifact would also affect the truncated (onlapping) reflections.

5.2. Seismic Evidence for Both Carbonate and Free Gas Within the Conduit

The carbonate crust that formed at shallow sedimentary depth, currently buried at 91 mbsf, is a distinctive layer-conforming, normal polarity, bright spot with a diameter of several hundreds of meters (Figure 3c). In clear contrast, the two bright but scattered high amplitude anomalies in the lower half of the conduit are unconformable to the surrounding strata (Figures 3a and 3b), which is common for shallow gas-charged sediments (Bünz et al., 2012). Additionally, reflections directly beneath the bright spots exhibit signs of frequency/wavenumber attenuation, typically associated with the presence of free gas (e.g., Castanga et al., 2003). A polarity reversal of the seismic reflections would provide additional evidence for free gas, because the velocity decrease caused by free gas leads to a negative reflection coefficient. However, the chaotic and patchy reflection pattern makes polarity identification ambiguous. Based on their reflection characteristics, and the observed decrease of frequency/wavenumber beneath, we interpret the bright spots as ascending gas fronts within the conduit.

There are several interesting observations regarding the ascending gas fronts. First, the gas fronts are only observed in the deeper half of the gas conduit. Second, the upper gas front accumulates directly beneath a buried mound (Figure 6b). Considering this limited distribution, these observations perhaps suggest plugged vents and temporary entrapment of gas. This scenario is possible because the flanks and top of buried mounds are often associated with more consolidated and compacted sediments that might partially trap gas during its ascent through the gas conduit (Koch et al., 2016; Loher et al., 2018). Gas hydrate-filled fractures under buried carbonates have been documented at a dormant seep site a few tens of kilometers to the west of Formosa Ridge (Wang et al., 2018), indicating that free gas can migrate vertically along fractures well into the hydrate stability zone before becoming trapped. There is no direct seismic evidence for compacted sediment in these parts of the gas conduit (i.e., directly above the gas fronts). However, we cannot rule out the possibility that small-scale fluid migration features are concealed due to decreasing image quality at depth.

5.3. The Evolution of Seepage

5.3.1. Episodic Gas Release From the Sub-BGHSZ Reservoir

Present day gas seepage at Formosa Ridge indicates that gas has accumulated beneath the BGHSZ to a critical thickness whereby the total gas pressure overcomes the horizontal effective stress, which ultimately has led to hydraulic fracturing and the propagation of vertical gas conduits to the seafloor that release gas into the ocean (e.g., Crutchley et al., 2021; Flemings et al., 2003; Tréhu et al., 2004a). Gas conduit development can influence gas hydrate formation, water column chemistry and the seabed ecosystem (e.g., Levin, 2005; Milkov et al., 2005; Valentine, 2011). Ongoing gas seepage at the present day requires that the flux of gas to the base of the gas conduit keeps pace with the flux of gas through the gas conduit to the seafloor—that is, a steady state system of gas supply and gas release, so that that the critical thickness of the reservoir is achieved and also sustained over long periods. These periods are obviously sufficiently long (thousands of years) to result in the formation of extensive carbonate deposits. The distinct intervals with free gas-related high amplitude anomalies suggest that gas seepage is intermittent throughout the geological history of the gas conduit. That is, the existence of buried mounds within the gas conduit points to distinct phases of gas seepage (i.e., 298 $\pm$ 213 ka, 220 $\pm$ 116 ka, and 183 $\pm$ 70 ka BP) and dormant periods between the active phases (Figure 6). Additionally, contemporary episodic gas migration events are suggested by the two separated gas fronts imaged within the conduit (Figure 3). Given that the activity of the gas conduit depends on the balance between the gas-water capillary pressure derived from the sub-BGHSZ gas reservoir and the effective horizontal stress at the BGHSZ (e.g., Crutchley et al., 2021; Flemings et al., 2003; Tréhu et al., 2004a), periods of dormancy may occur either due to a reduction of the thickness of the sub-BGHSZ gas reservoir or an increase of the overburden thickness. As such, there are several potential explanations for why the conduit goes in and out of active phases of gas flow, including changes in gas flux to the BGHSZ from below, rapid drainage of gas during fracturing events, and pronounced seafloor sedimentation that leads to an increase in the effective pressure at the BGHSZ. We discuss these possible processes below.

Long-period intermittent seepage could occur due to irregular gas flux from below the BGHSZ that leads to dynamic pressure fluctuations around the threshold of sub-BGHSZ critical pressure. For example, a rapid reduction or even complete cessation in gas flux to the BGHSZ would mean that the gas reservoir cannot be sustained at the critical thickness and the hydraulic fractures would close. Gas might still migrate slowly upward through the pore space (capillary flow), which would lead to a gradual reduction in thickness of the gas reservoir. Without capillary gas flow, the gas reservoir would stay at just below the critical thickness—the gas is trapped within the reservoir and the thickness is not quite enough to overcome the horizontal effective stress (i.e., to form hydraulic fractures). For the system to enter a subsequent phase of gas seepage through the conduit, gas flux would need to increase again to fill the sub-BGHSZ reservoir to the critical thickness. We cannot perceive of any reasonable geological mechanism to cause such significant changes in gas flux from below.

Alternatively, it is possible that intermittent seepage occurs in a system with constant gas flux toward the BGHSZ. One possible mechanism would be if gas drainage through the conduit occurs at a significantly higher flux than the gas flux into the sub-BGHSZ gas reservoir from below. This process could result in a relatively rapid reduction in the column of sub-BGHSZ free gas, such that it is no longer at the critical thickness required for hydraulic fracturing. Such a mechanism has been modeled numerically as part of sensitivity testing of gas conduit formation (Elger et al., 2018), but we are unaware of it being observed in nature. Elger et al.'s (2018) results indicated it would require a relatively small sub-BGHSZ gas volume (e.g., a layer constrained free gas reservoir) rather than a broader and larger sub-BGHSZ free gas volume.

A further alternative is a model where episodic gas seepage on long time scales is primarily the result of rapid seafloor sedimentation. We prefer this model for its simplicity and because it is consistent with the laterally varying depositional patterns coinciding with conduit formation times (Figure 7). It also does not require any change in gas flux from below. A conceptual model for this evolution of seepage is shown in Figure 8. Hydraulic fracturing will occur when the gas pressure converges on the horizontal effective stress (Figure 8b). The state of the system is in equilibrium - free gas is continually being supplied from below, and it is being vented off at the top. Periods of dormancy are associated with periods where there is enhanced seafloor sedimentation (e.g., sediment wave deposition). This gradually thickens the GHSZ to a thickness that means the effective horizontal stress at the BGHSZ becomes higher than the gas pressure from the free gas reservoir (Figure 8c). As a result, hydraulic fracturing and flow through the conduit shut down. When sedimentation rates at the seafloor slow down again (or arrest), the free gas reservoir will steadily fill up (due to the steady flux of free gas from below) to a new, thicker critical thickness required to overcome the greater horizontal effective stress at the BGHSZ (Figure 8d). Seepage will continue again in steady equilibrium until the next time when there is rapid seafloor sedimentation that "outpaces" the effect of gas supply from below.

Episodic seepage has been suggested previously for most of the seeps in the northern SCS (Chen et al., 2019; Feng et al., 2018; Liang et al., 2017). Geochemical results from these studies demonstrated that seepage timing mostly correlates with times of sea-level lowstands or periods when the sea-level was falling (Feng et al., 2018; and references therein), although climate-driven increase in temperature (Chen et al., 2019) and dynamic mass wasting (e.g., turbidity currents; Liang et al., 2017) have also been suggested as possible triggers for hydrate dissociation and active methane seepage at some sites. Interestingly, results from seabed carbonates at Formosa Ridge, that yielded ages younger than 10 ka BP, do not corroborate the hypothesis of hydrostatic pressure variation from sea level change being the primary factor for seepage (Feng & Chen, 2015). Our results complement these previous studies by extending Formosa Ridge's seepage history beyond 300,000 years ago. Unfortunately, the uncertainties for our age estimates are too large to verify with certainty whether temperature or sea-level stand variations have contributed to triggering gas seepage during the long history of the conduit. We note, however, since the area was under the influence of a strong laterally varying erosion and deposition patterns (Figure 7), reduction in overburden from rapid seafloor erosion could trigger an onset of gas seepage (i.e., the opposite of the scenario where deposition leads to dormancy). The reduction in effective stress at the BGHSZ could then be overcome by an underlying free gas reservoir, as proposed conceptually by Bangs et al. (2010). Future studies are required to evaluate these different drivers of episodic methane discharge, in addition to possible changes in gas flux from below (Figure 8), at this deep-water gas hydrate system. Deeper sediment coring would be required to generate a more accurate chronology of past methane seepage, thus providing additional constraints on local and regional drivers of long-term seepage.

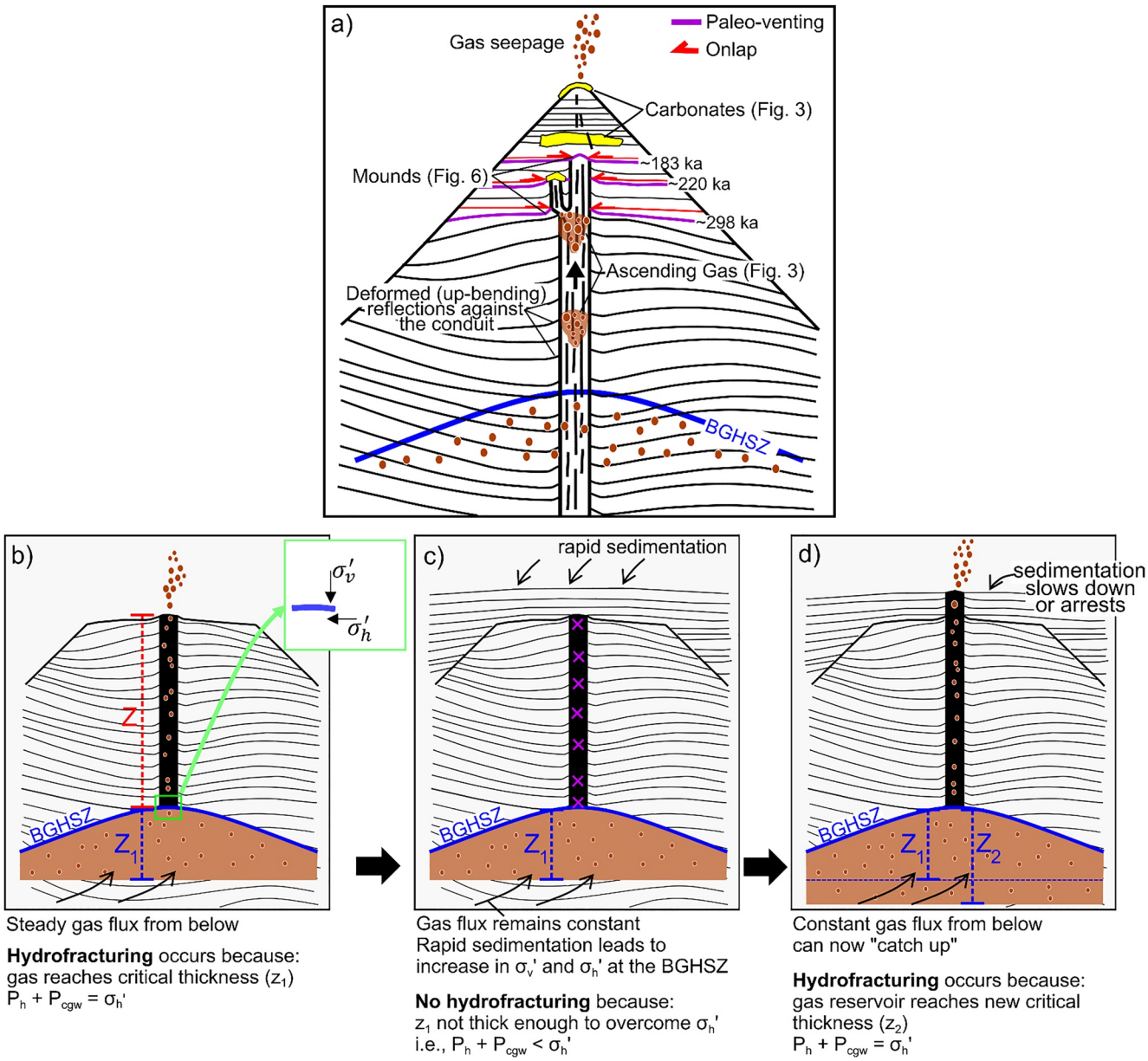

Figure 8. (a) Sketch of interpreted gas migration scenario beneath Formosa ridge, based on the present-day geometry in Figure 7a. Interpreted flow paths (arrows). BGHSZ = base of gas hydrate stability zone. Network of fractures is the link between the gas hydrate system at depth and methane seepage at the surface. Dense layers of carbonate are assumed to act as permeability barriers/capillary seals and encourage arrest or deflection of gas migration pathways. (b) Our interpretation of the first phase of gas seepage. The free gas reservoir is at a critical thickness (z_1) where gas pressure at the top of the reservoir equals the ambient horizontal effective stress (σ'_h) (e.g., Flemings et al., 2003). This enables vertical hydraulic fracturing and development of the gas conduit. Activity of the gas conduit depends on the balance between the gas-water capillary pressure (P_{cgw}) derived from the sub-BGHSZ gas reservoir and the effective horizontal stress (σ'_h) at the BGHSZ. P_h is hydrostatic pressure, σ'_v is the effective vertical stress. (c) Interpretation of a phase of dormancy, where rapid seafloor sedimentation leads to an increase in effective stress at the BGHSZ, thus the threshold for hydraulic fracturing. (d) Our interpretation of a subsequent phase of gas seepage, where hydraulic fracturing resumes once the free gas reservoir has filled up again to achieve the critical thickness (z_2) required for gas pressure to overcome the increased effective horizontal stress.

5.3.2. Stratigraphic and Structural Controls on Fluid Flow

Studies of gas hydrate systems and seep sites elsewhere have demonstrated the importance of stratigraphic control on fluid migration and gas accumulation, in particular the intersection of prominent carrier beds with the BGHSZ (e.g., Crutchley et al., 2013; Flemings et al., 2003; Tréhu et al., 2004b). Such studies have argued that these intersections form the locus for excess pressure accumulation at the BGHSZ. At Formosa Ridge, these processes

could be manifested in varying conduit locations throughout the different depth levels. This is because, with each progressive period of fluid expulsion, the BGHSZ depth is expected to have equilibrated in accordance with the developing contourite drift geometry, thereby causing new preferred loci for conduit development and varying intersection points between sedimentary structures (that constrain fluid flow) and the BGHSZ.

We have shown that in the shallow sedimentary section (<500 mbsf) fluid flow focusing toward the gas hydrate system seems to be primarily driven by stratigraphy rather than by structural elements, for example, fluid migration along the contourite deposit that intersects the BSR (Figure 5b). Concurrently, we have shown that the conduit has had a spatially persistent planform geometry during its growth period between 300,000 and 127,000 years ago (Figure 4). Since pre-existing fractures are presumably mechanically weaker than the undeformed host sediment, it seems likely that any sub-BGHSZ gas would prefer to use pre-existing fluid migration pathways than form new ones at different loci for gas conduit development (Cartwright et al., 2007). Therefore, we conclude that the stratigraphic architecture may not necessarily play a long-term role in terms of defining the source point of focused flow at the BGHZ. This suggests that stratigraphic architecture played an important role in defining the initial location of the conduit, but that subsequent seepage episodes will exploit the exiting fractures rather than forming new conduits at different locations. Together with continued gas flow into the sub-BGHSZ reservoir, this would explain the long-term spatial stability of the seep location.

5.3.3. Shallow Carbonates Control Seep Distribution at the Seafloor

The gas hydrate and methane seep system at south Hydrate Ridge, off Oregon, is comparable with the Formosa Ridge seep system in terms of the morphology and spatial distribution of the carbonate deposits. In both cases, permeable stratigraphic layers act as pathways that focus fluid flow toward the ridge, and together with a well-defined network of fractures, reveal the link between the gas hydrate system at depth and methane seepage at the seafloor (Tréhu et al., 2004b). Contemporary fluid expulsion at the seafloor, however, is not vertically aligned to these underlying fractures; instead, dense layers of carbonate are assumed to act as seals and encourage arrest or deflection of fluid migration pathways. At Hydrate Ridge, a pronounced carbonate structure, the Pinnacle, overlying the fractures and located several hundred meters west of the ridge's summit, has led to a lateral displacement of seepage activity toward the summit (Teichert et al., 2003). The Pinnacle was the first long-lived location of focused seepage that is a direct consequence of the underlying sedimentary architecture and its relationship to the BGHSZ (Crutchley et al., 2013; Tréhu et al., 2004b). However, after the fluid migration pathways self-sealed due to the carbonate and hydrate seals, the gas flow was deflected to the summit (Milkov et al., 2005) where active seepage has been documented (Kannberg et al., 2013). We interpret the Pinnacle as a modern analog of carbonate formation that formed in the shallow sediment section at Formosa Ridge, which is now buried at 91 mbsf. Similar to Hydrate Ridge, the carbonate deposits appears to hinder the upward migration of fluids during the final stages of ascent, as it deflects gas migration pathways toward the south, from which point the gas can migrate along the contourite layers toward the summit. Concurrently, fluids may also migrate vertically along fractures imaged in Figure 3b through the carbonate layers, if these pathways have not been clogged by hydrate formation (e.g., Wang et al., 2018). In any case, once the fluids have been diverted around the carbonate seal, they should be able to migrate freely toward the seafloor due to the increased gas buoyancy and decreasing lithostatic pressure (Talukder, 2012).

Overall, the results from the Formosa Ridge seep site demonstrate that on a local scale, and over long-time scales, multiple factors interact to determine where and when seepage occurs. We have shown how gas bypasses the hydrate stability zone and is vented at the seafloor through hydraulic fracturing. Concurrently, gas migration pathways can be redirected to the summit by shallow carbonates, which may influence the long-term seepage distribution at seafloor, thus playing an important role for sustaining seabed chemosynthetic biological communities. Our study further indicates that long-lived seeps may have intermittent seepage activity, and the frequency of events varies at not just short time scales (e.g., seasonal or tidal), but substantially longer scales (tens of thousands of years). Regional processes such as sea-level changes or bottom-water warming are not needed to trigger dissociation and seepage from sub-BGHSZ gas reservoirs. Instead, in a system with constant gas flux from below, changes in the GHSZ thickness due to rapid seafloor sedimentary processes may cause the conduit to go in and out of active phases of gas flow as they modify the effective horizontal stress at the BGHSZ. Since methane seepage plays an important role in seafloor biology and ocean chemistry (e.g., Biastoch et al., 2011; Boetius & Wenzhöfer, 2013; Levin et al., 2016), future studies should investigate how long-lived episodic seepage cycles might impact long-term ocean biogeochemistry.

6. Conclusions

Analysis of the 3D seismic data at Formosa Ridge enabled us to study the anatomy of a complex seep system in unprecedented detail. We have characterized the stratigraphic and structural framework of the gas conduit that are important to better understand the long-term evolution of fluid migration patterns through the GHSZ and into the ocean. Our five main conclusions are:

1. Gas has accumulated beneath the BGHSZ to a critical thickness that has led to hydraulic fracturing and the development of a sub-vertical gas conduit toward the seafloor and seabed morphological features (mounds). There are at least three episodes of seepage between 300 and 127 ka, evidenced by mounds within the conduit that are now buried.
2. Pulses (non steady-state) of upward gas migration may also occur at the present day, as indicated by two distinct gas accumulations imaged within the conduit. The irregularity of gas migration events is signified by their distinct depth separation.
3. The leak point at the BGHSZ (from where the gas migrates along fractures toward the seafloor) has been stable during the geological history of the conduit. Overpressured fluids presumably prefer to use pre-existing fractures from the first gas seepage phase rather than form new fracture networks at different locations.
4. Present-day gas seepage is not strictly vertical from the sub-BGHSZ reservoir toward the seafloor. Gas hydrate and carbonate precipitation in the shallow strata will cause the migration of flow conduits over time as gas migration pathways are blocked and flow is diverted laterally.
5. Past and present gas migration events can be driven by rapid sedimentary processes that modify the effective horizontal stress at the BGHSZ, thus the threshold for hydraulic fracturing. That is, during phases of increased deposition, the effective horizontal stress at the BGHSZ is higher than the gas pressure from the gas reservoir due to the gradually thickened GHSZ, which causes fractures to close. For the fractures to reopen, and a renewed phase of gas seepage to occur, the gas reservoir needs to fill up to a new critical thickness required for hydraulic fracturing.

Conflict of Interest

The authors declare no conflicts of interest relevant to this study.

Data Availability Statement

Seismic data from the Formosa Ridge are available through Berndt et al. (2019) (https://doi.pangaea.de/10.1594/PANGAEA.913192).

Acknowledgments
We thank the captain and crew of R/V Sonne for their help collecting the 3-D seismic data. We also thank IHS for access to Kingdom interpretation software within the academic licensing program. We are grateful to two anonymous reviewers and the Editor (Douglas Schmitt) who provided thorough and helpful comments that significantly improved this manuscript. This project is supported by MOST via grant number 111-2811-M-001-035. This is IESAS contribution 2410 and TEC contribution 00178. Open Access funding enabled and organized by Projekt DEAL.

References

Bangs, N. L., Hornbach, M. J., Moore, G. F., & Park, J. O. (2010). Massive methane release triggered by seafloor erosion offshore southwestern Japan. *Geology*, *38*(11), 1019–1022. https://doi.org/10.1130/g31491.1

Berndt, C., Chi, W. C., Jegen, M., Lebas, E., Crutchley, G., Muff, S., et al. (2019). Tectonic controls on gas hydrate distribution off SW Taiwan. *Journal of Geophysical Research: Solid Earth*, *124*(2), 1164–1184. https://doi.org/10.1029/2018jb016213

Biastoch, A., Treude, T., Rüpke, L. H., Riebesell, U., Roth, C., Burwicz, E. B., et al. (2011). Rising Arctic Ocean temperatures cause gas hydrate destabilization and ocean acidification. *Geophysical Research Letters*, *38*(8). https://doi.org/10.1029/2011gl047222

Boetius, A., & Wenzhöfer, F. (2013). Seafloor oxygen consumption fuelled by methane from cold seeps. *Nature Geoscience*, *6*(9), 725–734. https://doi.org/10.1038/ngeo1926

Bohrmann, G., Ahrlich, F., Bergenthal, M., Berndt, C., Chen, J.-N., Chen, S.-C., et al. (2019). MeBo200 methane hydrate drillings Southwest of Taiwan, TaiDrill, cruise No. SO266/1, 15 October - 18 November 2018. *Kaohsiung (Taiwan) - Kaohsiung (Taiwan)*. https://doi.org/10.48433/cr_so266_1

Bünz, S., Polyanov, S., Vadakkepuliyambatta, S., Consolaro, C., & Mienert, J. (2012). Active gas venting through hydrate-bearing sediments on the Vestnesa Ridge, offshore W-Svalbard. *Marine Geology*, *332*, 189–197. https://doi.org/10.1016/j.margeo.2012.09.012

Cartwright, J., Huuse, M., & Aplin, A. (2007). Seal bypass systems. *AAPG Bulletin*, *91*(8), 1141–1166. https://doi.org/10.1306/04090705181

Castagna, J. P., Sun, S., & Siegfried, R. W. (2003). Instantaneous spectral analysis: Detection of low-frequency shadows associated with hydrocarbons. *The Leading Edge*, *22*(2), 120–127. https://doi.org/10.1190/1.1559038

Chen, F., Wang, X., Li, N., Cao, J., Bayon, G., Peckmann, J., et al. (2019). Gas hydrate dissociation during sea-level highstand inferred from U/Th dating of seep carbonate from the South China Sea. *Geophysical Research Letters*, *46*(23), 13928–13938. https://doi.org/10.1029/2019gl085643

Chopra, S., & Marfurt, K. J. (2007). *Seismic attributes for prospect identification and reservoir characterization*. Society of Exploration Geophysicists and European Association of Geoscientists and Engineers.

Crutchley, G. J., Berndt, C., Geiger, S., Klaeschen, D., Papenberg, C., Klaucke, I., et al. (2013). Drivers of focused fluid flow and methane seepage at south Hydrate Ridge, offshore Oregon, USA. *Geology*, *41*(5), 551–554. https://doi.org/10.1130/g34057.1

Crutchley, G. J., Mountjoy, J. J., Hillman, J. I. T., Turco, F., Watson, S., Flemings, P. B., et al. (2021). Upward-doming zones of gas hydrate and free gas at the bases of gas chimneys, New Zealand's Hikurangi margin. *Journal of Geophysical Research: Solid Earth*, *126*(9), e2020JB021489. https://doi.org/10.1029/2020jb021489

Elger, J., Berndt, C., Rüpke, L., Krastel, S., Felix, G., & Geissler, W. H. (2018). Submarine slope failures due to pipe structure formation. *Nature Communications*, *9*, 715. https://doi.org/10.1038/s41467-018-03176-1

Fang, Y., Flemings, P. B., Daigle, H., Phillips, S. C., Meazell, P. K., & You, K. (2020). Petrophysical properties of the Green Canyon Block 955 hydrate reservoir inferred from reconstituted sediments: Implications for hydrate formation and production. *AAPG Bulletin*, *104*(9), 1997–2028. https://doi.org/10.1306/01062019165

Feng, D., & Chen, D. (2015). Authigenic carbonates from an active cold seep of the northern South China sea: New insights into fluid sources and past seepage activity. *Deep Sea Research Part II: Topical Studies in Oceanography*, *122*, 74–83. https://doi.org/10.1016/j.dsr2.2015.02.003

Feng, D., Qiu, J. W., Hu, Y., Peckmann, J., Guan, H., Tong, H., et al. (2018). Cold seep systems in the South China Sea: An overview. *Journal of Asian Earth Sciences*, *168*, 3–16. https://doi.org/10.1016/j.jseaes.2018.09.021

Flemings, P. B., Liu, X., & Winters, W. J. (2003). Critical pressure and multiphase flow in Blake Ridge gas hydrates. *Geology*, *31*(12), 1057–1060. https://doi.org/10.1130/g19863.1

Fongngern, R., Chi, W. C., Berndt, C., & Mohrig, D. (2022). Recognition and three-dimensional characteristics of ancient supercritical flow bedforms on a submarine slope: An example from the South China Sea. *Sedimentology*. https://doi.org/10.1111/sed.13002

Haeckel, M., Suess, E., Wallmann, K., & Rickert, D. (2004). Rising methane gas bubbles form massive hydrate layers at the seafloor. *Geochimica et Cosmochimica Acta*, *68*(21), 4335–4345. https://doi.org/10.1016/j.gca.2004.01.018

Han, X., Suess, E., Liebetrau, V., Eisenhauer, A., & Huang, Y. (2014). Past methane release events and environmental conditions at the upper continental slope of the south China sea: Constraints by seep carbonates. *International Journal of Earth Sciences*, *103*(7), 1873–1887. https://doi.org/10.1007/s00531-014-1018-5

Hornbach, M. J., Bangs, N. L., & Berndt, C. (2012). Detecting hydrate and fluid flow from bottom simulating reflector depth anomalies. *Geology*, *40*(3), 227–230. https://doi.org/10.1130/g32635.1

Hustoft, S., Bünz, S., & Mienert, J. (2010). Three-dimensional seismic analysis of the morphology and spatial distribution of chimneys beneath the Nyegga pockmark field, offshore mid-Norway. *Basin Research*, *22*(4), 465–480.

Judd, A., & Hovland, M. (2009). *Seabed fluid flow: The impact on geology, biology and the marine environment*. Cambridge University Press.

Kannberg, P. K., Tréhu, A. M., Pierce, S. D., Paull, C. K., & Caress, D. W. (2013). Temporal variation of methane flares in the ocean above Hydrate Ridge, Oregon. *Earth and Planetary Science Letters*, *368*, 33–42. https://doi.org/10.1016/j.epsl.2013.02.030

Koch, S., Berndt, C., Bialas, J., Haeckel, M., Crutchley, G., Papenberg, C., et al. (2016). Gas-controlled seafloor doming. *Geology*, *43*(7), 571–574.

Levin, L. A. (2005). Ecology of cold seep sediments: Interactions of fauna with flow, chemistry and microbes. In *Oceanography and marine biology* (pp. 11–56). CRC Press.

Levin, L. A., Baco, A. R., Bowden, D. A., Colaco, A., Cordes, E. E., Cunha, M. R., et al. (2016). Hydrothermal vents and methane seeps: Rethinking the sphere of influence. *Frontiers in Marine Science*, *3*, 72. https://doi.org/10.3389/fmars.2016.00072

Liang, Q., Hu, Y., Feng, D., Peckmann, J., Chen, L., Yang, S., et al. (2017). Authigenic carbonates from newly discovered active cold seeps on the northwestern slope of the South China Sea: Constraints on fluid sources, formation environments, and seepage dynamics. *Deep Sea Research Part I: Oceanographic Research Papers*, *124*, 31–41. https://doi.org/10.1016/j.dsr.2017.04.015

Liebetrau, V., Eisenhauer, A., & Linke, P. (2010). Cold seep carbonates and associated cold-water corals at the Hikurangi margin, New Zealand: New insights into fluid pathways, growth structures and geochronology. *Marine Geology*, *272*(1–4), 307–318. https://doi.org/10.1016/j.margeo.2010.01.003

Liu, J., Haeckel, M., Rutqvist, J., Wang, S., & Yan, W. (2019). The mechanism of methane gas migration through the gas hydrate stability zone: Insights from numerical simulations. *Journal of Geophysical Research: Solid Earth*, *124*(5), 4399–4427. https://doi.org/10.1029/2019jb017417

Liu, X., & Flemings, P. B. (2006). Passing gas through the hydrate stability zone at southern Hydrate Ridge, offshore Oregon. *Earth and Planetary Science Letters*, *241*(1–2), 211–226. https://doi.org/10.1016/j.epsl.2005.10.026

Loher, M., Marcon, Y., Pape, T., Römer, M., Wintersteller, P., Dos Santos Ferreira, C., et al. (2018). Seafloor sealing, doming, and collapse associated with gas seeps and authigenic carbonate structures at Venere mud volcano, Central Mediterranean. *Deep Sea Research Part I: Oceanographic Research Papers*, *137*, 76–96. https://doi.org/10.1016/j.dsr.2018.04.006

Milkov, A. V., Claypool, G. E., Lee, Y. J., & Sassen, R. (2005). Gas hydrate systems at Hydrate Ridge offshore Oregon inferred from molecular and isotopic properties of hydrate-bound and void gases. *Geochimica et Cosmochimica Acta*, *69*(4), 1007–1026. https://doi.org/10.1016/j.gca.2004.08.021

Nyman, S. L., Nelson, C. S., & Campbell, K. A. (2010). Miocene tubular concretions in East Coast basin, New Zealand: Analogue for the subsurface plumbing of cold seeps. *Marine Geology*, *272*(1–4), 319–336. https://doi.org/10.1016/j.margeo.2009.03.021

Passaro, S., Tamburrino, S., Vallefuoco, M., Tassi, F., Vaselli, O., Giannini, L., et al. (2016). Seafloor doming driven by degassing processes unveils sprouting volcanism in coastal areas. *Scientific Reports*, *6*(1), 1–10. https://doi.org/10.1038/srep22448

Petersen, C. J., Bünz, S., Hustoft, S., Mienert, J., & Klaeschen, D. (2010). High-resolution P-Cable 3D seismic imaging of gas chimney structures in gas hydrated sediments of an Arctic sediment drift. *Marine and Petroleum Geology*, *27*(9), 1981–1994. https://doi.org/10.1016/j.marpetgeo.2010.06.006

Planke, S., Eriksen, F. N., Berndt, C., Mienert, J., & Masson, D. G. (2009). P-Cable high-resolution seismic. *Oceanography*, *22*(1), 85. https://doi.org/10.5670/oceanog.2009.09

Plaza-Faverola, A., Bünz, S., & Mienert, J. (2011). Repeated fluid expulsion through sub-seabed chimneys offshore Norway in response to glacial cycles. *Earth and Planetary Science Letters*, *305*(3–4), 297–308. https://doi.org/10.1016/j.epsl.2011.03.001

Sawyer, D. E., Flemings, P. B., Dugan, B., & Germaine, J. T. (2009). Retrogressive failures recorded in mass transport deposits in the Ursa Basin, Northern Gulf of Mexico. *Journal of Geophysical Research*, *114*. https://doi.org/10.1029/2008jb006159

Shipley, T. H., Houston, M. H., Buffler, R. T., Shaub, F. J., Mcmillen, K. J., Laod, J. W., & Worzel, J. L. (1979). Seismic evidence for widespread possible gas hydrate horizons on continental slopes and rises. *AAPG Bulletin*, *63*(12), 2204–2213.

Sloan, E. D., Jr., & Koh, C. A. (2007). *Clathrate hydrates of natural gases*. CRC Press.

Suess, E., Torres, M., Bohrmann, G., Collier, R. W., Collier, R. W., Rickert, D., et al. (2001). *Dynamics of sea floor hydrate at Hydrate Ridge*. In C. Paull (Ed.) (Vol. 124, pp. 87–98). AGU Monograph.

Talukder, A. R. (2012). Review of submarine cold seep plumbing systems: Leakage to seepage and venting. *Terra Nova*, *24*(4), 255–272. https://doi.org/10.1111/j.1365-3121.2012.01066.x

Taner, M. T. (1997). Seismic trace attributes and their projected use in prediction of rocks properties and seismic facies, Technical report: Rock Solid Images.

Taylor, M. H., Dillon, W. P., & Pecher, I. A. (2000). Trapping and migration of methane associated with the gas hydrate stability zone at the Blake Ridge Diapir: New insights from seismic data. *Marine Geology*, *164*, 79–89. https://doi.org/10.1016/s0025-3227(99)00128-0

Teichert, B. M. A., Eisenhauer, A., Bohrmann, G., Haase-Schramm, A., Bock, B., & Linke, P. (2003). U/Th systematics and ages of authigenic carbonates from Hydrate Ridge, Cascadia margin: Recorders of fluid flow variations. *Geochimica et Cosmochimica Acta*, *67*(20), 3845–3857. https://doi.org/10.1016/s0016-7037(03)00128-5

Tong, H., Feng, D., Cheng, H., Yang, S., Wang, H., Min, A. G., et al. (2013). Authigenic carbonates from seeps on the northern continental slope of the south China sea: New insights into fluid sources and geochronology. *Marine and Petroleum Geology*, *43*, 260–271.

Tréhu, A. M., Flemings, P. B., Bangs, N. L., Chevallier, J., Gràcia, E., Johnson, J. E., et al. (2004a). Feeding methane vents and gas hydrate deposits at south Hydrate Ridge. *Geophysical Research Letters*, *31*(23). https://doi.org/10.1029/2004gl021286

Tréhu, A. M., Long, P. E., Torres, M. E., Bohrmann, G. R. R. F., Rack, F. R., Collett, T. S., et al. (2004b). Three-dimensional distribution of gas hydrate beneath southern Hydrate Ridge: Constraints from ODP Leg 204. *Earth and Planetary Science Letters*, *222*(3–4), 845–862. https://doi.org/10.1016/s0012-821x(04)00219-5

Valentine, D. L. (2011). Emerging topics in marine methane biogeochemistry. *Annual Review of Marine Science*, *3*, 147–171. https://doi.org/10.1146/annurev-marine-120709-142734

Wang, X., Liu, B., Qian, J., Zhang, X., Guo, Y., Su, P., et al. (2018). Geophysical evidence for gas hydrate accumulation related to methane seepage in the Taixinan Basin, South China Sea. *Journal of Asian Earth Sciences*, *168*, 27–37. https://doi.org/10.1016/j.jseaes.2017.11.011